Perfectly Matched Layers Used as Absorbing Boundaries in a Three-dimensional FDTD Code

David M. Hockanson

Abstract

The Finite-Difference Time-Domain (FDTD) method is a powerful tool for modeling open region problems. However, current methods of mesh truncation, such as Mur absorbing boundaries, enlarge the computational domain undesirably and provide nominal accuracy. The development of a new absorbing boundary is reviewed which increase the effectiveness of the FDTD analysis method. The Perfectly Matched Layer (PML) absorbing boundaries developed by Berenger provide an order of magnitude increase in accuracy compared to Mur absorbing boundaries. The PML boundaries function independent of frequency and angle of incidence. PML requires a smaller extension of the computational domain than Mur absorbing boundaries. However, the computation time necessary for calculating field values in the PML boundary is higher than the time required for free-space field computations. The PML absorbing boundaries are implemented in the UMR FDTD code and comparisons between results using Mur absorbing boundaries and PML absorbing boundaries are made for two geometries.

Keywords

FDTD, Absorbing Boundaries, PML

I. Introduction

THE Finite-Difference Time-Domain (FDTD) analysis method is well documented and is not discussed here. The reader is referred to [1], [2], and [3] for information on FDTD.

The FDTD analysis method models open region problems well, provided that the computational domain can be truncated with minimal reflections. Early attempts at absorbing boundaries involved placing lossy media far from all scatterers. However, this method was very inefficient as it required very thick layers and the absorbing characteristics of the media were only effective for normally incident waves. More accurate techniques, such as Mur's absorbing boundaries [4], were developed in the late 1970's which involved enforcing outgoing wave equations at the boundary of the computational domain. Mur's absorbing boundaries, however, do not absorb waves with angles of incidence far from normal and must be placed some distance (usually one-half to one wavelength) from all scatterers. Mur's absorbing boundaries exhibit reflection coefficients between -40 dB and -50 dB [5].

A new method has been developed for very effective absorbing boundaries in two-dimensions [6] and extended to three-dimensions [7] using Perfectly Matched Layers (PMLs). The PMLs absorb outgoing waves of any frequency and any angle of incidence. PML boundaries can achieve reflection coefficients below -60 dB. Chew and Weedon's development of three-dimensional PML boundaries will be presented.

Implementation of the PML boundaries is discussed and demonstrated using the UMR FDTD code [8]. A short dipole in free-space and a dipole antenna in free-space are modeled with PML and Mur absorbing boundaries, alternately. The results using the two different boundary methods are compared for accuracy and efficiency.

II. Theory

The Perfectly Matched Layer (PML) absorbing boundary establishes a lossy layer at the edge of the computational domain which has no reflections regardless of angle of incidence or frequency. The lossy PML is truncated by a perfect electric conductor (pec) which encloses the computational domain in three dimensions. The absorbing layer is anisotropic with special electric and magnetic loss terms. By choosing a particular level of loss the absorbing boundary can absorb outgoing waves with reflection coefficients of less than -60dB.

The investigation begins with a rectangular coordinate system which is stretched along the axes and can be represented by the modified del operator [9]

$$\nabla_s = \hat{\mathbf{x}}\frac{1}{s_x}\frac{\partial}{\partial x} + \hat{\mathbf{y}}\frac{1}{s_y}\frac{\partial}{\partial y} + \hat{\mathbf{z}}\frac{1}{s_z}\frac{\partial}{\partial z}. \tag{1}$$

D. M. Hockanson is with the Department of Electrical Engineering at the University of Missouri–Rolla (UMR) in Rolla, MO 65401, USA. E-mail: hockanso@umr.edu

Maxwell's equations in a general source-free medium in a time-harmonic form can then be expressed as

$$\begin{aligned} \nabla_e \times \vec{\mathbf{E}} &= -j\omega\mu\vec{\mathbf{H}} && (2)\\ \nabla_h \times \vec{\mathbf{H}} &= j\omega\epsilon\vec{\mathbf{E}} && (3)\\ \nabla_h \cdot \epsilon\vec{\mathbf{E}} &= \rho && (4)\\ \nabla_e \cdot \mu\vec{\mathbf{H}} &= 0, && (5) \end{aligned}$$

where Equations (4) and (5) can be derived from Equations (2) and (3). The operators are defined as

$$\begin{aligned} \nabla_e &\equiv \hat{\mathbf{x}}\frac{1}{e_x}\frac{\partial}{\partial x} + \hat{\mathbf{y}}\frac{1}{e_y}\frac{\partial}{\partial y} + \hat{\mathbf{z}}\frac{1}{e_z}\frac{\partial}{\partial z} && (6)\\ \nabla_h &\equiv \hat{\mathbf{x}}\frac{1}{h_x}\frac{\partial}{\partial x} + \hat{\mathbf{y}}\frac{1}{h_y}\frac{\partial}{\partial y} + \hat{\mathbf{z}}\frac{1}{h_z}\frac{\partial}{\partial z}, && (7) \end{aligned}$$

where $\vec{\mathbf{E}}$ and $\vec{\mathbf{H}}$ are the electric and magnetic field vectors, respectively, μ and ϵ are the permeability and permittivity, respectively and ρ is the volumetric charge density. The time dependence is $e^{j\omega t}$. Note that if $h_x = h_y = h_z \equiv 1 - j\frac{\sigma}{\omega}$ then Equation (3) becomes

$$\begin{aligned} \nabla_h \times \vec{\mathbf{H}} &= \\ \frac{1}{1-j\frac{\sigma}{\omega}}\nabla \times \vec{\mathbf{H}} &= j\omega\vec{\mathbf{E}} \\ &\Rightarrow \\ \nabla \times \vec{\mathbf{H}} &= j\omega\vec{\mathbf{E}} + \sigma\vec{\mathbf{E}}. && (8) \end{aligned}$$

Equation (8) is Ampere's law in an electrically lossy medium.

For a general plane wave with a spatial functional dependence of the form $e^{-j\vec{\mathbf{k}}\cdot\vec{\mathbf{r}}}$, where

$$\vec{\mathbf{k}} \equiv \hat{\mathbf{x}}k_x + \hat{\mathbf{y}}k_y + \hat{\mathbf{z}}k_z \quad (9)$$

and $|\vec{\mathbf{k}}| = \omega\sqrt{\mu\epsilon} \equiv k$, Equations (2)–(5) become

$$\begin{aligned} \vec{\mathbf{k_e}} \times \vec{\mathbf{E}} &= \omega\mu\vec{\mathbf{H}} && (10)\\ \vec{\mathbf{k_h}} \times \vec{\mathbf{H}} &= -\omega\epsilon\vec{\mathbf{E}} && (11)\\ \vec{\mathbf{k_h}} \cdot \epsilon\vec{\mathbf{E}} &= \rho && (12)\\ \vec{\mathbf{k_e}} \cdot \mu\vec{\mathbf{H}} &= 0, && (13) \end{aligned}$$

where $\vec{\mathbf{k_e}} \equiv \hat{\mathbf{x}}\frac{k_x}{e_x} + \hat{\mathbf{y}}\frac{k_y}{e_y} + \hat{\mathbf{z}}\frac{k_z}{e_z}$ and $\vec{\mathbf{k_h}} \equiv \hat{\mathbf{x}}\frac{k_x}{h_x} + \hat{\mathbf{y}}\frac{k_y}{h_y} + \hat{\mathbf{z}}\frac{k_z}{h_z}$. Therefore, $\vec{\mathbf{k_e}}\times$ Equation (11) yields

$$\begin{aligned} \vec{\mathbf{k_e}} \times \vec{\mathbf{k_h}} \times \vec{\mathbf{H}} &= -\omega\epsilon\vec{\mathbf{k_e}} \times \vec{\mathbf{E}} \\ &\Rightarrow \\ \vec{\mathbf{k_e}} \times \vec{\mathbf{k_h}} \times \vec{\mathbf{H}} &= -\omega^2\mu\epsilon\vec{\mathbf{H}} = -k^2\vec{\mathbf{H}}. && (14) \end{aligned}$$

Using the vector identity $\vec{\mathbf{A}} \times \vec{\mathbf{B}} \times \vec{\mathbf{C}} = \vec{\mathbf{B}}(\vec{\mathbf{A}} \cdot \vec{\mathbf{C}}) - \vec{\mathbf{C}}(\vec{\mathbf{A}} \cdot \vec{\mathbf{B}})$, Equation (14) can be written as

$$\begin{aligned} \vec{\mathbf{k_h}}\underbrace{(\vec{\mathbf{k_e}} \cdot \vec{\mathbf{H}})}_{0} - \vec{\mathbf{H}}(\vec{\mathbf{k_e}} \cdot \vec{\mathbf{k_h}}) &= -k^2\vec{\mathbf{H}} && (15)\\ &\Rightarrow \\ \vec{\mathbf{k_e}} \cdot \vec{\mathbf{k_h}} &= k^2. && (16) \end{aligned}$$

Performing the dot product in Equation (16) yields

$$\frac{k_x^2}{e_x h_x} + \frac{k_y^2}{e_y h_y} + \frac{k_z^2}{e_z h_z} = k^2, \quad (17)$$

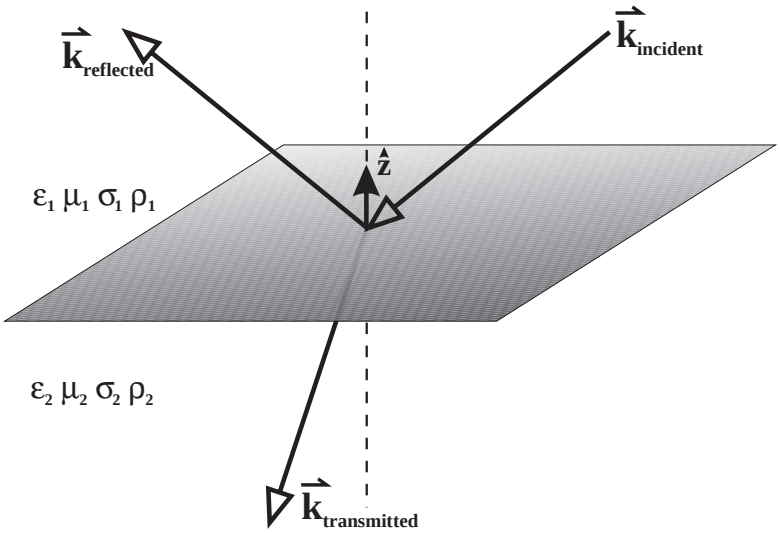

Fig. 1. Geometry of a wave incident on an interface with an arbitrary angle of incidence.

which is the equation for an ellipse with solution

$$k_x = k\sqrt{e_x h_x}\sin\theta\cos\phi \tag{18}$$
$$k_y = k\sqrt{e_y h_y}\sin\theta\sin\phi \tag{19}$$
$$k_z = k\sqrt{e_z h_z}\cos\theta, \tag{20}$$

where (θ,ϕ) are spherical reference angles. If $\vec{\mathbf{k_e}} = \vec{\mathbf{k_h}}$ then $\vec{\mathbf{k_h}} \perp \vec{\mathbf{H}}$, the magnitude of Equation (11) can be expressed as

$$\left|\vec{\mathbf{k_h}} \times \vec{\mathbf{H}}\right| = \left|\vec{\mathbf{k_h}}\right|\left|\vec{\mathbf{H}}\right| = \omega\epsilon\left|\vec{\mathbf{E}}\right|.$$

For $\vec{\mathbf{k_h}} = \vec{\mathbf{k_e}}$, $\left|\vec{\mathbf{k_h}}\right| = k = \omega\sqrt{\mu\epsilon}$ which yields

$$\frac{\left|\vec{\mathbf{E}}\right|}{\left|\vec{\mathbf{H}}\right|} = \sqrt{\frac{\mu}{\epsilon}} = \eta. \tag{21}$$

In the remaining theoretical discussion, a PML medium will be a material such that $\vec{\mathbf{k_e}} = \vec{\mathbf{k_h}}$.

A matched interface of PML media is indicated by a reflection coefficient which is zero independent of frequency or angle of incidence. The necessary relationship between two PML media for null reflections can be determined by letting a plane wave be incident on an interface between two PML media normal to $\hat{\mathbf{z}}$ as depicted in Fig. 1. For TE_z polarization the electric fields associated with the rays in Fig. 1 can be expressed as

$$\vec{\mathbf{E_i}} = \vec{\mathbf{E_o}} e^{-j\vec{\mathbf{k_i}}\cdot\vec{\mathbf{r}}} \tag{22}$$
$$\vec{\mathbf{E_r}} = R^{TE}\vec{\mathbf{E_o}} e^{-j\vec{\mathbf{k_r}}\cdot\vec{\mathbf{r}}} \tag{23}$$
$$\vec{\mathbf{E_t}} = T^{TE}\vec{\mathbf{E_o}} e^{-j\vec{\mathbf{k_t}}\cdot\vec{\mathbf{r}}}, \tag{24}$$

assuming no depolarization. For the TE_z case, $\vec{\mathbf{k_i}}\cdot\vec{\mathbf{E_i}} = 0$ and $\vec{\mathbf{E_o}}$ is entirely in the $\hat{\mathbf{x}}-\hat{\mathbf{y}}$ plane. The boundary condition on the tangential components of the electric field can be expressed as

$$\left(\vec{\mathbf{E_o}} e^{-j\vec{\mathbf{k_i}}\cdot\vec{\mathbf{r}}} + R^{TE}\vec{\mathbf{E_o}} e^{-j\vec{\mathbf{k_r}}\cdot\vec{\mathbf{r}}}\right)\Big|_{z=0} = T^{TE}\vec{\mathbf{E_o}} e^{-j\vec{\mathbf{k_t}}\cdot\vec{\mathbf{r}}}\Big|_{z=0}. \tag{25}$$

Phase matching along the boundary constrains $k_{i_x} = k_{r_x} = k_{t_x}$ and $k_{i_y} = k_{r_y} = k_{t_z}$. The boundary condition on the electric field is then expressed as

$$1 + R^{TE} = T^{TE}. \tag{26}$$

Since the interface is between two PML media, let $\vec{\mathbf{k_e}} = \vec{\mathbf{k_h}} \equiv \vec{\mathbf{k_s}}$ for reference. Equation (10) yields

$$\vec{\mathbf{H_i}} = \frac{1}{\omega\mu_1}\vec{\mathbf{k_{s_i}}} \times \vec{\mathbf{E_o}} e^{-j\vec{\mathbf{k_i}}\cdot\vec{\mathbf{r}}} \tag{27}$$

$$\vec{\mathbf{H_r}} = \frac{R^{TE}}{\omega\mu_1}\vec{\mathbf{k_{s_r}}} \times \vec{\mathbf{E_o}} e^{-j\vec{\mathbf{k_r}}\cdot\vec{\mathbf{r}}} \tag{28}$$

$$\vec{\mathbf{H_t}} = \frac{T^{TE}}{\omega\mu_2}\vec{\mathbf{k_{s_t}}} \times \vec{\mathbf{E_o}} e^{-j\vec{\mathbf{k_t}}\cdot\vec{\mathbf{r}}} \tag{29}$$

The boundary conditions on the magnetic field constrain

$$\vec{\mathbf{z}} \times \vec{\mathbf{H_i}} + \vec{\mathbf{z}} \times \vec{\mathbf{H_r}} = \vec{\mathbf{z}} \times \vec{\mathbf{H_t}}. \tag{30}$$

Using the aforementioned vector identity yields

$$\begin{aligned} \vec{\mathbf{z}} \times \vec{\mathbf{k_s}} \times \vec{\mathbf{E_o}} &= \vec{\mathbf{k_s}} \overbrace{(\vec{\mathbf{z}} \cdot \vec{\mathbf{E_o}})}^{0} - \vec{\mathbf{E_o}}(\vec{\mathbf{z}} \cdot \vec{\mathbf{k_s}}) \\ &= -\vec{\mathbf{E_o}}(\vec{\mathbf{z}} \cdot \vec{\mathbf{k_s}} \qquad (31) \\ &= -\vec{\mathbf{E_o}}\frac{k_z}{s_z} \qquad (32) \end{aligned}$$

The boundary condition on the magnetic field can then be expressed as

$$\frac{1}{\mu_1}\frac{k_{i_z}}{s_{1_z}} + \frac{1}{\mu_1}\frac{k_{r_z}}{s_{1_z}}R^{TE} = \frac{1}{\mu_2}\frac{k_{t_z}}{s_{2_z}}T^{TE} \tag{33}$$

The phase matching condition and Equation (9) further stipulate that $k_{z_i} = -k_{z_r} \equiv k_{z_1}$. For convenience define $k_{z_t} \equiv k_{z_2}$. The boundary condition on the magnetic field can then be expressed as

$$\frac{k_{z_1}}{s_{z_1}}(1 - R^{TE}) = T^{TE}\frac{k_{z_2}}{s_{z_2}} \tag{34}$$

Letting the permeability in both PML media be the same, and simultaneously solving Equations (34) and (26) results in the reflection coefficient which is expressed as

$$R^{TE} = \frac{k_{z_1}s_{z_2} - k_{z_2}s_{z_1}}{k_{z_1}s_{z_2} + k_{z_2}s_{z_1}}. \tag{35}$$

The TM_z problem yields an identical reflection coefficient ($R^{TE} = R^{TM} \equiv R$).

Substituting Equation (20) into Equation (35) yields

$$R = \frac{k_1 s_{z_1} s_{z_2}\cos\theta_1 - k_2 s_{z_2} s_{z_1}\cos\theta_2}{k_1 s_{z_1} s_{z_2}\cos\theta_1 + k_2 s_{z_2} s_{z_1}\cos\theta_2} \tag{36}$$

If $\epsilon_1 = \epsilon_2$ and $\mu_1 = \mu_2$, then $k_1 = k_2$ and the reflection coefficient can be reduced to

$$R = \frac{\cos\theta_1 - \cos\theta_2}{\cos\theta_1 + \cos\theta_2} \tag{37}$$

Equations (18) and (19) in conjunction with the phase matching requirements $k_{x_1} = k_{x_2}$ and $k_{y_1} = k_{y_2}$ yields

$$k_1 s_{x_1}\sin\theta_1\cos\phi_1 = k_2 s_{x_2}\sin\theta_2\cos\phi_2 \tag{38}$$

$$k_1 s_{y_1}\sin\theta_1\sin\phi_1 = k_2 s_{y_2}\sin\theta_2\sin\phi_2 \tag{39}$$

Restricting $s_{x_1} = s_{x_2}$ and $s_{y_1} = s_{y_2} \Rightarrow \theta_1 = \theta_2$ and $\phi_1 = \phi_2$ and therefore

$$R = 0. \tag{40}$$

In general for planar PML interfaces in rectangular coordinate systems with normal $\hat{\mathbf{x_1}}$ and unit vectors $\hat{\mathbf{x_2}}$ and $\hat{\mathbf{x_3}}$ parallel to the surface

$$s_{x_{2medium1}} = s_{x_{2medium2}} \tag{41}$$
$$s_{x_{3medium1}} = s_{x_{3medium2}} \tag{42}$$
$$s_{x_{1medium1}} \neq s_{x_{1medium2}}, \tag{43}$$

for an interface exhibiting no incident field reflections.

Knowing the requirements for s_i is not congenial to FDTD analysis methods because the development was made using time-harmonic equations. Meaningful media properties can be determined by reinstating the time-dependence of Maxwell's equations. equations for a PML media. Equations (2) and (3) for PML media can be expressed as

$$\nabla_s \times \vec{\mathbf{E}} = -j\omega\mu\vec{\mathbf{H}} \tag{44}$$
$$\nabla_s \times \vec{\mathbf{H}} = j\omega\epsilon\vec{\mathbf{E}}, \tag{45}$$

where $\nabla_s \equiv \frac{1}{s_x}\frac{\partial}{\partial x} + \frac{1}{s_y}\frac{\partial}{\partial y} + \frac{1}{s_z}\frac{\partial}{\partial z}$. Expanding Equation (44) yields

$$\begin{aligned} -j\omega\mu\left(H_x\hat{\mathbf{x}} + H_y\hat{\mathbf{y}} + H_z\hat{\mathbf{z}}\right) &= \frac{1}{s_x}\left(\frac{\partial E_y}{\partial x}\hat{\mathbf{x}} - \frac{\partial E_z}{\partial x}\hat{\mathbf{y}}\right) \\ &+\frac{1}{s_y}\left(\frac{\partial E_z}{\partial y}\hat{\mathbf{x}} - \frac{\partial E_x}{\partial y}\hat{\mathbf{z}}\right) \\ &+\frac{1}{s_z}\left(\frac{\partial E_x}{\partial z}\hat{\mathbf{y}} - \frac{\partial E_y}{\partial z}\hat{\mathbf{x}}\right). \end{aligned} \tag{46}$$

Equation (45) can be expanded in a similar form. The electric and magnetic field components can be decomposed as

$$\begin{array}{ll} E_x = E_{xy} + E_{xz} & H_x = H_{xy} + H_{xz} \\ E_y = E_{yx} + E_{yz} & H_y = H_{yx} + H_{yz} \\ E_z = E_{zx} + E_{zy} & H_z = H_{zy} + H_{zx} \end{array} \tag{47}$$

Twelve scalar equations can then be written of the form

$$-j\omega\mu H_{xz} = \frac{1}{s_y}\frac{\partial E_z}{\partial y}. \tag{48}$$

Define $s_y \equiv 1 - j\frac{\rho_y}{\omega\mu}$ ($s_y \equiv 1 - j\frac{\sigma_y}{\omega\epsilon}$ for E_{xz} equation), where ρ is the magnetic resistivity and σ is the electric conductivity, and rewrite Equation (48) as

$$-j\omega\mu H_{xz} - \rho_y H_{xz} = \frac{\partial E_z}{\partial y}. \tag{49}$$

Re-instating the time dependence in Equation (49) yields a scalar time-dependent field equation for PML media

$$\mu\frac{\partial H_{xz}}{\partial t} + \rho_y H_{xz} = -\frac{\partial E_z}{\partial y} \tag{50}$$

The conditions for a PML interface in this form for a interface with $\hat{\mathbf{x_1}}$ normal and $\hat{\mathbf{x_2}}$ and $\hat{\mathbf{x_3}}$ parallel to the interface are

$$\rho_{x_1 medium1} \neq \rho_{x_1 medium2} \tag{51}$$
$$\rho_{x_2 medium1} = \rho_{x_2 medium2} \tag{52}$$
$$\rho_{x_3 medium1} = \rho_{x_3 medium2} \tag{53}$$

where $\epsilon_{medium1} = \epsilon_{medium2}$, $\mu_{medium1} = \mu_{medium2}$, and $\frac{\rho}{\mu} = \frac{\sigma}{\epsilon}$ in each PML medium. Eleven more equations can be developed in the same manner and all twelve are given below for reference.

$$\begin{array}{ll} \mu\frac{\partial H_{xy}}{\partial t} + \rho_z H_{xy} = +\frac{\partial E_y}{\partial z} & \mu\frac{\partial H_{xz}}{\partial t} + \rho_y H_{xz} = -\frac{\partial E_z}{\partial y} \\ \mu\frac{\partial H_{yx}}{\partial t} + \rho_z H_{yx} = -\frac{\partial E_x}{\partial z} & \mu\frac{\partial H_{yz}}{\partial t} + \rho_x H_{yz} = +\frac{\partial E_z}{\partial x} \\ \mu\frac{\partial H_{zx}}{\partial t} + \rho_y H_{zx} = +\frac{\partial E_x}{\partial y} & \mu\frac{\partial H_{zy}}{\partial t} + \rho_x H_{zy} = -\frac{\partial E_y}{\partial x} \end{array} \tag{54}$$

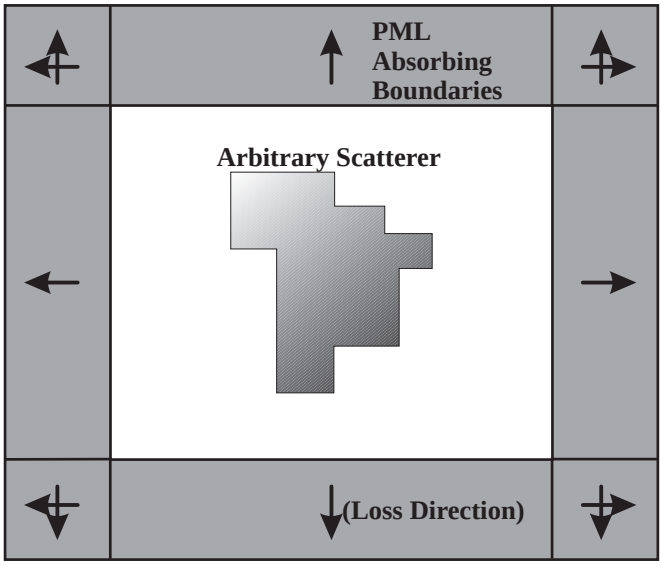

Fig. 2. Two-dimensional view of an open region problem bounded by PMLs. The arrows indicate the direction of loss.

$$\begin{array}{ll} \epsilon\frac{\partial E_{xy}}{\partial t}+\sigma_z E_{xy}=-\frac{\partial H_y}{\partial z} & \epsilon\frac{\partial E_{xz}}{\partial t}+\sigma_y E_{xz}=+\frac{\partial H_z}{\partial y} \\ \epsilon\frac{\partial E_{yx}}{\partial t}+\sigma_z E_{yx}=+\frac{\partial H_x}{\partial z} & \epsilon\frac{\partial E_{yz}}{\partial t}+\sigma_x E_{yz}=-\frac{\partial H_z}{\partial x} \\ \epsilon\frac{\partial E_{zx}}{\partial t}+\sigma_y E_{zx}=-\frac{\partial H_x}{\partial y} & \epsilon\frac{\partial E_{zy}}{\partial t}+\sigma_x E_{zy}=+\frac{\partial H_y}{\partial x} \end{array} \tag{55}$$

III. FDTD Implementation

An open region problem can be modeled in FDTD by bounding the domain with a PML. The PML is truncated by either a pec or Mur absorbing boundaries. However, if Mur absorbing boundaries are used, the correct phase velocity must be known a priori which can be difficult to ascertain. Pec boundaries are simple to implement and when used with a PML with adequate loss function adequately.

The computational domain of interest contacts PML's along faces which have loss only along the direction of the normal. The faces overlap along edges which have loss in two directions, and the edges overlap at corners having loss in three directions. Fig. 2 shows a two dimensional view of a domain truncated with PML boundaries.

Ideally the PML would be implemented with a high, constant loss term. However, large step changes in loss in an FDTD grid contribute undesirable numerical reflections [6]. To prevent numerical reflections, the electrical conductivity (and therefore the magnetic resistivity) must be ramped to a maximum value. The maximum value can be found by choosing a reflection coefficient that is acceptable for a given application. A wave with normal incidence on a PML with thickness d which is truncated by a pec must travel through the medium twice. For a conductivity with a quadratic ramp

$$\sigma(r)=\sigma_{max}\left(\frac{r}{d}\right)^2, \tag{56}$$

the reflection coefficient can be expressed as

$$R=e^{-2\frac{1}{\epsilon c}\int_0^d \sigma_{max}\left(\frac{r}{d}\right)^2 dr}=e^{-\frac{2\sigma_{max}d}{\epsilon c3}} \tag{57}$$

If R was desired to be approximately -60 dB, then $\sigma_{max}d\approx 0.0275$ for a PML matched to free-space. The speed of light in the PML medium is or can be approximated to be the speed of light in free-space [6].

The differential equation is discretized at a single point in time and space for every element in the equation. Therefore, PML field update equations are discretized using the value of the conductivity at the same location as the electric field component in the equation, or the value of the resistivity at the location of a magnetic field component. However, for materials with high loss, care must be given to maintain the diffusion stability criterion. By using exponential differencing, the diffusion stability criterion is met regardless of the value of loss [1]. A discretized PML time-update

equation using central differencing can then be expressed as

$$H_{xy}^{n+\frac{1}{2}}(i,j+\frac{1}{2},k+\frac{1}{2}) = e^{-\rho_z \frac{\Delta t}{\mu}} H_{xy}^{n-\frac{1}{2}}(i,j+\frac{1}{2},k+\frac{1}{2}) + \frac{1-e^{-\rho_z \frac{\Delta t}{\mu}}}{\rho_z \Delta z}\left(E_y^n(i,j+\frac{1}{2},k+1) - E_y^n(i,j+\frac{1}{2},k)\right) \quad (58)$$

IV. Results

The PML absorbing boundaries were implemented in the UMR FDTD code. Two geometries were modeled to compare the results using PML boundary conditions and Mur second-order boundary conditions. The first simulation modeled of a short dipole in free-space. The field results from simulations using each boundary technique were compared. The second geometry was a dipole antenna. The input impedance for the center-fed dipole antenna was computed with mesh truncation provided by second order Mur absorbing boundaries and PML boundaries.

A short dipole source was placed in a computational domain one wavelength cubed. The domain was discretized with cubic cells of dimension $\Delta l = \frac{\lambda}{20}$ and a differential time element $\Delta t = \frac{\Delta l}{2c}$. A $\hat{\mathbf{z}}$-polarized, $1\frac{A}{cm^2}$ electric current density source was placed at Node (6,6,6). The Mur second-order absorbing boundaries were placed one half wavelength (ten cells) from the computational domain. The PML boundaries were six cells thick and started four cells from the computational domain for a total extension of ten cells beyond the computational domain.

The electric field components were computed along a line through the source in the $\hat{\mathbf{x}}$-direction and are shown in Fig. 3. The values found above and below the source for E_x and E_y were averaged to provide the field values in the plane of the source, because E_x and E_y are not computed by the FDTD algorithm in the plane of the source. The agreement for E_z computed in the presence of the two different absorbing boundaries is very good. However, there are discrepancies for the computations of E_x and E_y using the two different absorbing boundaries. E_x and E_y should be zero in the plane of the source and are not because of numerical reflections from the absorbing boundaries. The PML boundaries were found to be more accurate by almost an order of magnitude. The disadvantage of the PML absorbing boundary was the PML boundaries require approximately three times the computational time to analyze the fields associated with a node inside the boundary layer than a free-space node.

Fig. 4 shows the dipole antenna that was numerically modeled by the UMR FDTD code. The domain was discretized with cubic cells of side dimension Δl and a differential time element $\Delta t = \frac{\Delta l}{2c}$. The antenna was center-fed by a voltage source of length Δl. Taflove's thin wire algorithm [10] was used to give the wire a radius of $a = 0.2\Delta l$, where a was the wire radius and Δl was the cell discretization. The input impedance was calculated for the antenna as a function of the ratio of length L, to wavelength λ, over the range $0.10 \leq \frac{L}{\lambda} \leq 2$. Other dimensions are given in terms of the ideal halfwave resonance wavelength, which is denoted by $\lambda_o \equiv 2L$.

The input impedance for the antenna was computed using Mur's second order absorbing boundaries placed one-half the longest wavelength of interest from the antenna and PML absorbing boundaries six cells thick placed four cells from the antenna. The input impedance results are shown in Fig. 5. The figure shows good agreement between the results for the two boundary conditions. The results with PML differ slightly at the lowest frequency point. The error may be attributed to the PML boundaries being too close to the antenna with respect to wavelength at that frequency, effectively loading the antenna. The primary advantage of the PML boundaries was that the simulation ran in approximately a tenth of the time required with the second-order Mur absorbing boundaries because less domain was required for the PML boundaries.

V. Conclusion

Perfectly Matched Layer (PML) absorbing boundaries were reviewed and implemented in the UMR FDTD code. The code modeled two geometries with computational domains truncated with PML absorbing boundaries and Mur second-order absorbing boundaries, alternately. The first geometry involved a short electric dipole in free-space. The results with the PML absorbing boundaries were an order of magnitude better than the results for the same problem using Mur absorbing boundaries. However, the computations for a PML node require three times as much time per time-step than

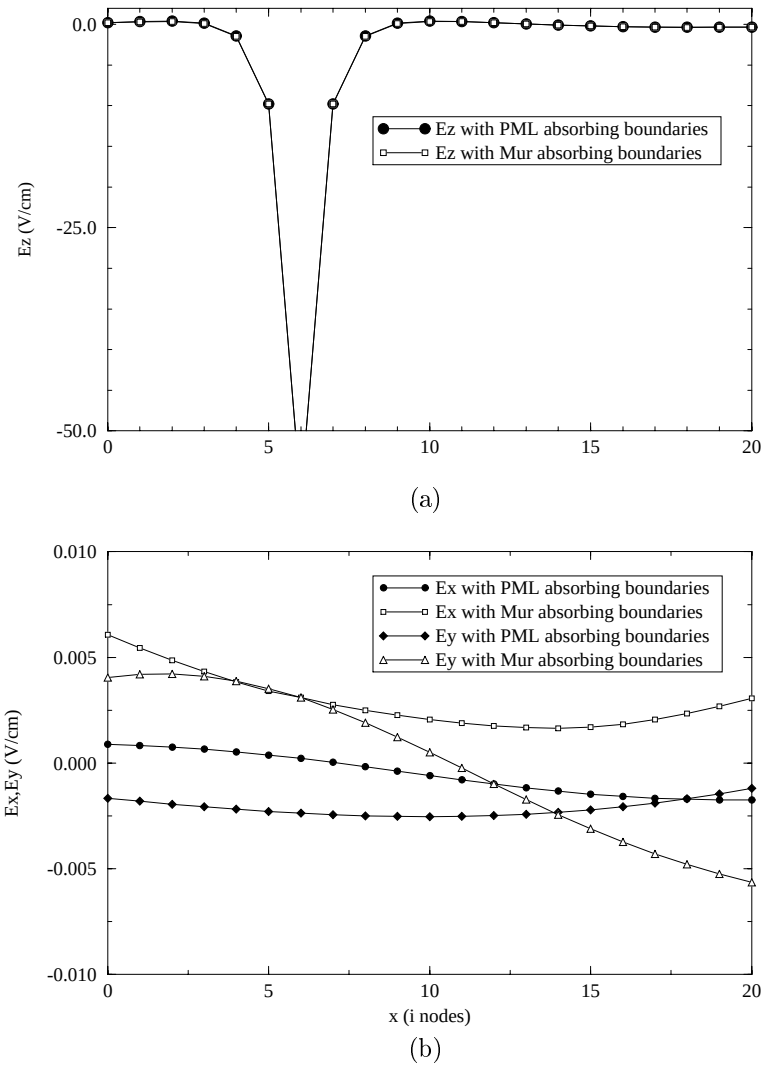

Fig. 3. Results for the short dipole in free-space along a line through the source in the $\hat{\mathbf{x}}$-direction for (a) E_z and (b) E_x and E_y using PML and Mur absorbing boundaries.

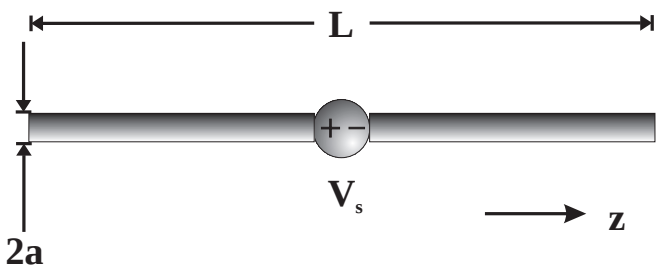

Fig. 4. The geometry of the dipole antenna model.

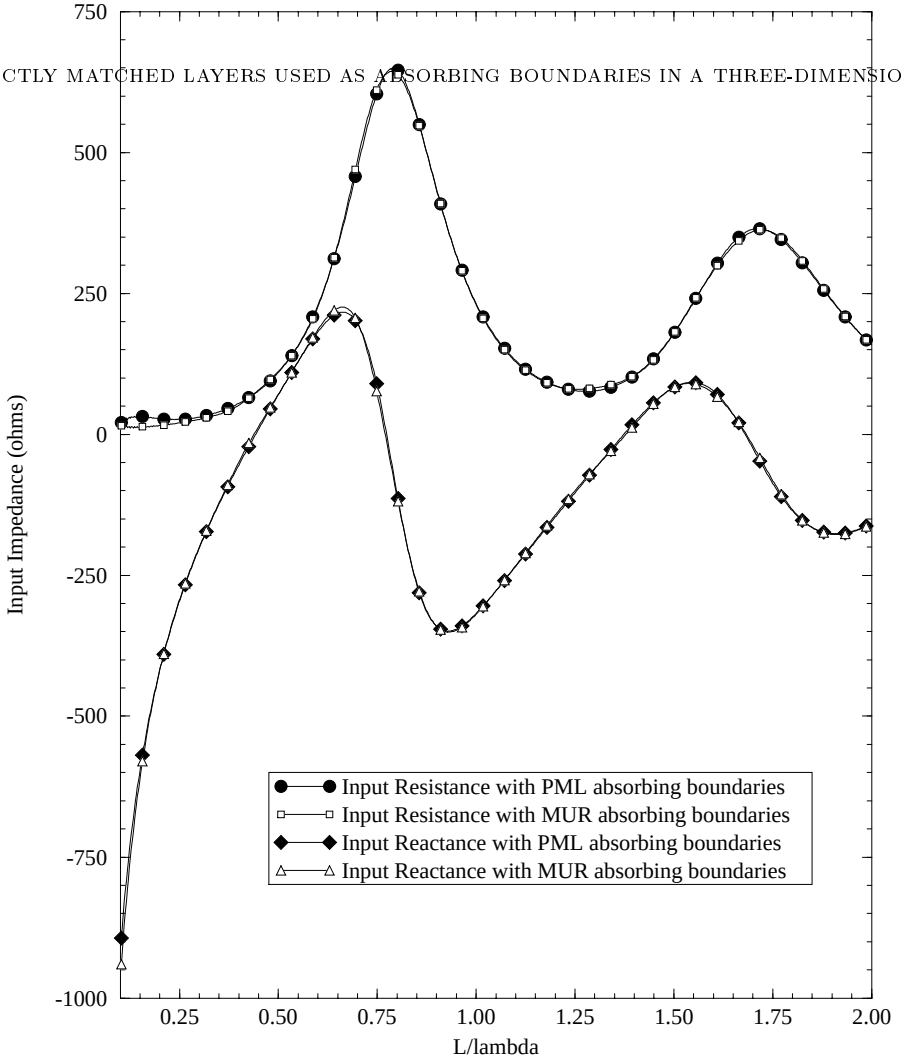

Fig. 5. Input impedance results for a dipole antenna with the domain truncated by Mur's second order boundary conditions, and a PML boundary six cells thick.

the field computations for a free-space node. The last geometry was a very thin, center-fed dipole antenna in free-space. The input impedance was calculated for a mesh truncated with Mur absorbing boundaries and then PML absorbing boundaries. The results showed good agreement, however the case with the PML absorbing boundaries was completed in less than twenty percent of the time necessary for the input impedance calculations using Mur absorbing boundaries. Mur absorbing boundaries must be placed at least a half-wavelength from all scatterers. The computational domain for problems employing fine spatial discretization may be largely white space necessary for the Mur absorbing boundaries. The PML boundaries were placed four cells from the scatterers regardless of discretization requiring a lower number of total nodes, which may offset the longer run-time necessary for PML nodes.

More simulations are required to determine the optimum location and thickness of the PML boundaries. However, the initial results are very encouraging. The greater accuracy provided to the FDTD analysis by the PML boundaries will permit FDTD modeling of geometries where accuracy is very important, such as aerospace applications. The PML boundaries increase the computational domain to a lesser degree than Mur absorbing boundaries for fine mesh discretization permitting more accurate models of geometries such as printed circuit boards.

VI. Conjecture

The following statements are conjecture and no results or theory are given as support. The PML boundaries will probably work more accurately if placed a little farther away from the scatterer. Especially when the scatterers are expected to have highly reactive fields. For fine discretization, four cells may be in the near field and the PML will

absorb reactive fields which may consist of important information such as in the case of input impedance. Thicker PML walls allow a more gradual change of loss while allowing more loss overall and may prove to be worth the extra computational time and memory consumption. The thicker walls seemed to result in impedance calculations that were identical to the impedance results with Mur absorbing boundaries. The increase in memory required by PML is worth the time it can save for problems necessitating fine meshes. The value of the PML boundaries will be further evident when Gaussian pulse sources are implemented in the UMR FDTD code. The Mur absorbing boundaries may result in some "ringing" in the computational domain while the PML boundaries shoule absorb the outgoing pulse to the same degree over the whole spectrum.

References

[1] K. S. Kunz and R. J. Luebbers, *The Finite Difference Time Domain Method for Electromagnetics*, CRC Press, Boca Raton, Florida, 1993.

[2] K. Li, M. A. Tassoudji, R. T. Shin, and J.A. Kong, "Simulation of electromagnetic radiation and scattering using a finite-difference time-domain technique", *Computer Applications in Engineering Education*, vol. 1, pp. 45–63, September/October 1992.

[3] A. Taflove, "Review of the formulation and applications of the finite-difference time-domain method for numerical modeling of electromagnetic wave interactions with arbitrary structures", *Wave Motion*, vol. 10, pp. 547–582, April 1988.

[4] G. Mur, "Absorbing boundary conditions for the finite-difference approximation of the time-domain electromagnetic-field equations", *IEEE Transactions on Electromagnetic Compatiblity*, vol. 23, pp. 377–382, November 1981.

[5] D. S. Katz, E. T. Thiele, and A. Taflove, "Validation and extension to three dimensions of the Berenger PML absorbing boundary condition for FD-TD meshes", *IEEE Transactions on Antennas and Propagation*, Submitted 1994.

[6] J. P. Berenger, "A perfectly matched layer for the absorption of electromagnetic waves", *Journal of Computational Physics*, vol. 114, no. 2, pp. 185–200, 1994.

[7] W. C. Chew and W. H. Weedon, "A 3-D perfectly matched medium from modified Maxwell's equation with stretched coordinates", *Microelectronices and Optics Technical Letters*, accepted for publication September 1994.

[8] D. M. Hockanson, "The Finite-Difference Time-Domain Method and Applications in Electromagnetic Compatibility", Master's thesis, University of Missouri–Rolla, 1994.

[9] C. T. Thai, *Generalized Vector and Dyadic Analysis*, IEEE Press, New York, New York, 1992.

[10] A. Taflove, K. Umashankar, B. Beker, F. Harfoush, and K. Yee, "Detailed FD-TD analysis of electromagnetic fields penetrating narrow slots and lapped joints in thick conducting screens", *IEEE Transactions on Antennas and Propagation*, vol. 36, pp. 247–257, February 1988.